Nonlinear Effects on Charge Fractionalization in Critical Chains

Flávia B. Ramos,[1] Rodrigo G. Pereira,[2] Sebastian Eggert,[1] and Imke Schneider[1]
[1]Physics Department and Research Center OPTIMAS, University of Kaiserslautern-Landau, 67663 Kaiserslautern, Germany
[2]International Institute of Physics and Departamento de Física Teórica e Experimental, Universidade Federal do Rio Grande do Norte, Natal, RN, 59078-970, Brazil

(Received 7 June 2024; accepted 16 July 2024; published 22 August 2024)

We investigate the generic transport in a one-dimensional strongly correlated fermionic chain beyond linear response. Starting from a Gaussian wave packet with positive momentum on top of the ground state, we find that the numerical time evolution splits the signal into at least three distinct fractional charges moving with different velocities. A fractional left-moving charge is expected from conventional Luttinger liquid theory, but for the prediction of the two separate right-moving packets the nonlinearity of the dispersion must also be taken into account. This out-of-equilibrium protocol therefore allows a direct measurement of nonlinear interaction parameters, which also govern threshold singularities of dynamic response functions. The nonlinear Luttinger liquid theory also predicts the correct dynamics at low energies, where it agrees with the conventional Luttinger liquid. Moreover, at high energies, the wave packet dynamics reveals signatures of composite excitations containing two-particle bound states. Our results uncover a simple strategy to probe the nonlinear regime in time-resolved experiments in quantum wires and ultracold-atom platforms.

DOI: 10.1103/PhysRevLett.133.086502

Introduction—The fractionalization of a particle into a composite of emergent excitations is one of the most striking phenomena in quantum many-body systems. The effect is prevalent in critical one-dimensional (1D) systems, in which interactions inevitably lead to a departure from Fermi liquid behavior [1–3]. Within the paradigm of Luttinger liquid (LL) theory [4,5], the low-energy spectrum of 1D quantum fluids is described by bosonic collective modes with a linear dispersion relation. This theory predicts that electrons fractionalize into right- and left-moving excitations that carry interaction-dependent charges [6,7], as indeed observed in transport experiments in quantum wires [8–11]. In addition, signatures of LL behavior have been identified via spectroscopic techniques [12–17] and quantum simulations in ultracold-atom platforms [18–21].

Despite its impressive success, LL theory breaks down whenever finite-energy excitations and band curvature have to be taken into account [22]. To treat the effects of a nonlinear dispersion, more general techniques have been developed into what became known as the nonlinear Luttinger liquid (nLL) theory [23–27]. In particular, dynamic response functions exhibit characteristic threshold singularities that can be described by treating the modes with finite energy and momentum as mobile impurities coupled to the gapless modes [24]. The exponents associated with these singularities can be expressed in terms of scattering phase shifts and calculated exactly for integrable models [27–30]. In the time domain, the contributions from high-energy modes give rise to power-law-decaying temporal oscillations that dominate the long-time behavior [31]. Moreover, nonlinearities are predicted to lead to shock waves in the evolution of density and magnetization pulses [32–35].

While the nonlinear regime is accessible in experiments [36–39], direct tests of the threshold singularities predicted by nLL theory are hindered by the limited energy resolution or disorder-induced broadening of spectroscopic probes. In this Letter, we show that the effects of the high-energy excitation in nLL theory can be directly observed in an out-of-equilibrium protocol. We create a Gaussian wave packet with preselected momentum in a critical fermionic chain and simulate its evolution using the adaptive time-dependent density matrix renormalization group (tDMRG) [40]. Similar protocols have been used to demonstrate fractionalization and spin-charge separation in the low-energy regime [41–47]. Beyond the LL paradigm, the nonlinear dispersion leads to a splitting of the initial wave packet into three density humps that propagate with different velocities [48,49]. Here, we show that the time-evolved signal can be predicted by nLL theory, which in turn provides a quantitative measurement of the interaction between the high-energy particle and the low-energy modes. At lower fillings and higher energies, we discover fingerprints of two-particle bound states in the wave packet dynamics.

Model and protocol—We consider a spinless fermion model described by the Hamiltonian

$$H = \sum_{j=1}^{L} \left[-\frac{1}{2} \left(c_j^\dagger c_{j+1} + \text{H.c.} \right) + V n_j n_{j+1} \right], \qquad (1)$$

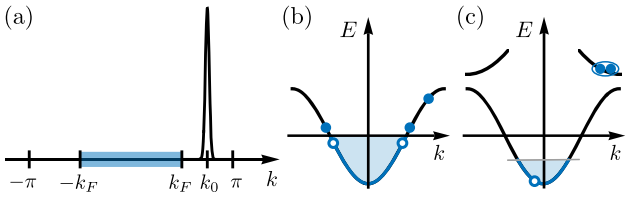

FIG. 1. (a) Gaussian wave packet in momentum space. (b) At half filling, the evolution is controlled by a particle above the Fermi level and low-energy particle-hole excitations. (c) At lower fillings, there are contributions from excitations with a hole and two particles in a high-energy bound-state band.

where c_j annihilates a fermion at site j of a chain with L sites, V is the strength of the nearest-neighbor interaction, and $n_j = c_j^\dagger c_j$ is the local density operator. We work at fixed number of fermions N, with average density $n = N/L$. For $V = 0$, the Hamiltonian can be diagonalized as $H_0 = \sum_k \varepsilon_0(k) c_k^\dagger c_k$, where $\varepsilon_0(k) = -\cos(k)$ is the dispersion relation of free fermions with momentum $k \in [-\pi, \pi]$, with lattice spacing set to unity. The ground state in this case is constructed by occupying single-particle states up to the Fermi momentum $k_F = \pi n$. More generally, the model in Eq. (1) is equivalent to the spin-1/2 XXZ chain and is exactly solvable via Bethe ansatz [50]. We focus on the parameter regime $0 \le V \le 1$, where the ground state $|\Psi_0\rangle$ of Eq. (1) is in a gapless phase described at low energies by LL theory [1].

We prepare an initial state given by

$$|\Psi(t=0)\rangle = A \sum_{j=1}^{L} e^{-\frac{(j-j_0)^2}{2\sigma_0^2}} e^{ik_0 j} c_j^\dagger |\Psi_0\rangle, \tag{2}$$

corresponding to a Gaussian wave packet centered at j_0, with variance $\sigma_0^2/2$ in real space and mean momentum k_0; here, A is a normalization constant. To add a particle with well-defined momentum, we choose $k_0 \in [k_F, \pi]$ with momentum uncertainty $\Delta k = 1/(\sqrt{2}\sigma_0)$; see Fig. 1(a). After the unitary evolution $|\Psi(t)\rangle = e^{-iHt}|\Psi(0)\rangle$, we measure the time-dependent local charge excess defined as

$$\rho_j(t) = \langle \Psi(t)|n_j|\Psi(t)\rangle - \langle \Psi_0|n_j|\Psi_0\rangle. \tag{3}$$

Free fermions—The local charge excess can be calculated exactly in the noninteracting case. For a finite chain with open boundary conditions, we obtain

$$\rho_j(t) = \left| \sum_{l=N+1}^{L} q(k_l) \sin(k_l j) e^{i\cos(k_l)t} \right|^2, \tag{4}$$

where $q(k) = [2A/(L+1)] \sum_{j=1}^{L} e^{-(j-j_0)^2/(2\sigma_0^2)} e^{ik_0 j} \sin(kj)$ and $k_l = l\pi/(L+1)$ with $l = 1, \ldots, L$. The result is analogous to the evolution of a Gaussian wave packet in the single-particle problem [51]. For small Δk, we can expand the dispersion as $\varepsilon_0(k) \approx \varepsilon_0(k_0) + u_0(k-k_0) + (1/2m_0)(k-k_0)^2$, where $u_0 = \sin(k_0)$ is the group velocity and $m_0 = [\cos(k_0)]^{-1}$ is the effective mass for momentum k_0. As a consequence, we observe a single packet that moves to the right with velocity u_0 and width growing as

$$\sigma(t)^2 \approx \sigma_0^2 \left(1 + \frac{t^2}{m_0^2 \sigma_0^4}\right). \tag{5}$$

We have used Eq. (4) to benchmark our tDMRG results, obtaining excellent agreement; see the Supplemental Material (SM) [52]. In all the numerics henceforth, we set $L = 300$, $j_0 = 150$, and $\sigma_0 = 14.5$. We keep up to 400 states per DMRG block and use the Trotter step $\delta t = 0.1$. The largest truncation error is of order 10^{-10}. The maximum time is set by stopping the simulations before the wave packets reach the chain boundaries.

nLL theory—We now turn to the interacting case. We seek to describe the dynamics using the framework of nLL theory [22]. In addition to the momentum k_0, we consider a mode expansion that includes the low-energy modes in the vicinity of the Fermi points [see Fig. 1(b)],

$$c_j^\dagger \sim e^{-ik_F x} \psi_R^\dagger(x) + e^{ik_F x} \psi_L^\dagger(x) + e^{-ik_0 x} d^\dagger(x). \tag{6}$$

In the absence of the high-energy particle created by $d^\dagger$, the low-energy modes are described by the LL Hamiltonian [1]

$$H_{\mathrm{LL}} = \frac{v}{2} \int dx \left[(\partial_x \varphi_R)^2 + (\partial_x \varphi_L)^2\right], \tag{7}$$

where v is the velocity of the low-energy modes and $\varphi_{R,L}(x)$ are the right- and left-moving components of the bosonic field obeying

$$[\partial_x \varphi_{R,L}(x), \varphi_{R,L}(x')] = \pm i\delta(x - x'). \tag{8}$$

The low-energy fermion fields can be bosonized in the form

$$\psi_{R,L}^\dagger(x) \sim e^{i\sqrt{\frac{\pi}{2K}}[(1\pm K)\varphi_R(x) + (1\mp K)\varphi_L(x)]}, \tag{9}$$

where K is the Luttinger parameter. Taking the continuum limit of Eq. (1) including the high-energy mode, we obtain the effective Hamiltonian

$$H_{\mathrm{nLL}} = H_{\mathrm{LL}} + \int dx\, d^\dagger(\varepsilon_{\mathrm{p}} - iu\partial_x) d + \frac{1}{\sqrt{2\pi K}} \int dx (\kappa_R \partial_x \varphi_R + \kappa_L \partial_x \varphi_L) d^\dagger d, \tag{10}$$

where ε_{p} and u are the renormalized energy and velocity, respectively, of the high-energy particle in the interacting

model. Note that the high-energy particle behaves as a mobile impurity [53,54] that interacts with the bosonic modes via the coupling constants $\kappa_{R,L}$.

The impurity mode can be decoupled from the bosonic fields by the unitary transformation $U = e^{-i\int(dx/\sqrt{2\pi K})(\gamma_R\varphi_R+\gamma_L\varphi_L)d^\dagger d}$, where $\gamma_{R,L} = \kappa_{R,L}/(v \mp u)$ are the right- and left-mover phase shifts. In the nLL, $\gamma_{R,L}$ govern all the space-time correlation functions of the system as well as the threshold singularities of dynamic response functions [24,27]. As we will see below, these nontrivial interaction parameters can be measured as fractional charges in our proposed out-of-equilibrium protocol.

We now proceed to calculate the fractional transport properties using the nLL theory. Up to irrelevant terms, the transformed Hamiltonian $\tilde{H}_{\mathrm{nLL}} = UH_{\mathrm{nLL}}U^\dagger$ becomes noninteracting [55]

$$\tilde{H}_{\mathrm{nLL}} = \frac{v}{2}\left[(\partial_x\tilde{\varphi}_R)^2 + (\partial_x\tilde{\varphi}_L)^2\right] + \tilde{d}^\dagger(\varepsilon_{\mathrm{p}} - iu\partial_x)\tilde{d}, \tag{11}$$

with

$$\partial_x\varphi_{R,L} = U^\dagger\partial_x\tilde{\varphi}_{R,L}U = \partial_x\tilde{\varphi}_{R,L} \pm \frac{\gamma_{R,L}}{\sqrt{2\pi K}}\tilde{d}^\dagger\tilde{d}, \tag{12}$$

$$d^\dagger = U^\dagger\tilde{d}^\dagger U = \tilde{d}^\dagger e^{\frac{i}{\sqrt{2\pi K}}\gamma_R\tilde{\varphi}_R}e^{\frac{i}{\sqrt{2\pi K}}\gamma_L\tilde{\varphi}_L}. \tag{13}$$

Note that an initial excitation $d^\dagger$ now consists of three parts: two vertex operators, $\mathcal{V}_{L,R}(x) = e^{(i/\sqrt{2\pi K})\gamma_{L,R}\tilde{\varphi}_{L,R}(x)}$, that excite low-energy modes $\tilde{\varphi}_{L,R}(x,t) = \tilde{\varphi}_{L,R}(x \pm vt)$ propagating with velocity $\pm v$ and a free particle $\tilde{d}^\dagger$ with velocity u, as schematically depicted in Fig. 1(b). The fractional charges of the three propagating parts can be measured with the charge density operator, which after rotation using Eq. (12) is given by

$$Q = \sqrt{\frac{K}{2\pi}}\partial_x(\tilde{\varphi}_L - \tilde{\varphi}_R) + \left(1 - \frac{\gamma_R + \gamma_L}{2\pi}\right)\tilde{d}^\dagger\tilde{d}. \tag{14}$$

By calculating the commutator using Eq. (8), we have

$$[Q(y), \mathcal{V}_{R,L}(x)] = \frac{\gamma_{R,L}}{2\pi}\mathcal{V}_{R,L}(x)\delta(x-y). \tag{15}$$

Thus, the right- and left-moving vertex operators carry fractional charges $n_{R,L} = (\gamma_{R,L}/2\pi)$ propagating with velocity $\pm v$. The remaining charge corresponding to the particle $\tilde{d}^\dagger$ is $n_I = 1 - n_R - n_L$ with velocity u.

In the tDMRG simulation, we use the Gaussian wave packet defined in Eq. (2); see Fig. 1(a). The propagation at half filling, $k_F = \pi/2$, is shown in Fig. 2(a). Note that all parameters are known in this case: $K = \pi/\{2[\pi - \arccos(V)]\}$, $v = \pi\sqrt{1-V^2}/[2\arccos(V)] = u/\sin(k_0)$, and *momentum-independent* phase shifts $\gamma_{R,L} = \pi(1-K)$ [27]. In all cases, we observe three fractional humps that move with the exact velocities and magnitudes predicted by the nLL theory. Remarkably, the shape of the low-energy wave packets is stable over the whole energy regime, showing coherence over long times as can be seen in Fig. 2(a). In addition, the variance of the high-energy hump, σ_h^2, grows in time according to Eq. (5) with an interaction-dependent effective mass; see Fig. 2(b). Therefore, the theoretical *ad hoc* prediction of exactly three parts in the mode expansion (6) surprisingly provides a robust prediction of a free stable fractional particle. See the SM [52] for more details on the fitting procedure.

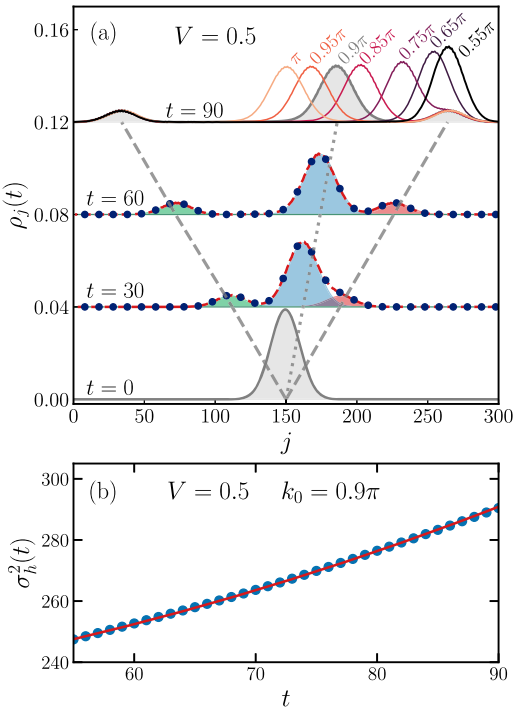

FIG. 2. Wave packet at half filling. (a) Snapshots of the averaged density profile for different times and $V = 0.5$. The time evolution is shown for $k_0 = 0.9\pi$. The gray dashed lines denote the light cone set by the velocity of the low-energy modes. The dotted line indicates the velocity of the high-energy particle. The shaded regions for the data $t = 30$ and 60 show the time-dependent Gaussian functions that reproduce the tDMRG results represented by the symbols. The red dashed lines are the sums of the Gaussian functions. For $t = 90$, we show density profiles for the values of k_0 indicated in the plot. (b) Variance of the high-energy hump vs t. The red solid line is a fit to our estimates using a quadratic function [52].

Here, spatial oscillations in the density with wave number $2k_F$ have been averaged out by taking the average $\rho_j(t)$ between two nearest-neighbor sites. They can be attributed to the staggered part of the density operator as discussed in the SM [52].

In our analysis, we have used a large set of different values of t, V, and k_0, which all show excellent agreement with the nLL theory. This implies that the nLL theory remarkably describes the *whole* energy regime covered by the Gaussian excitation with momentum $k_0 > k_F$. As

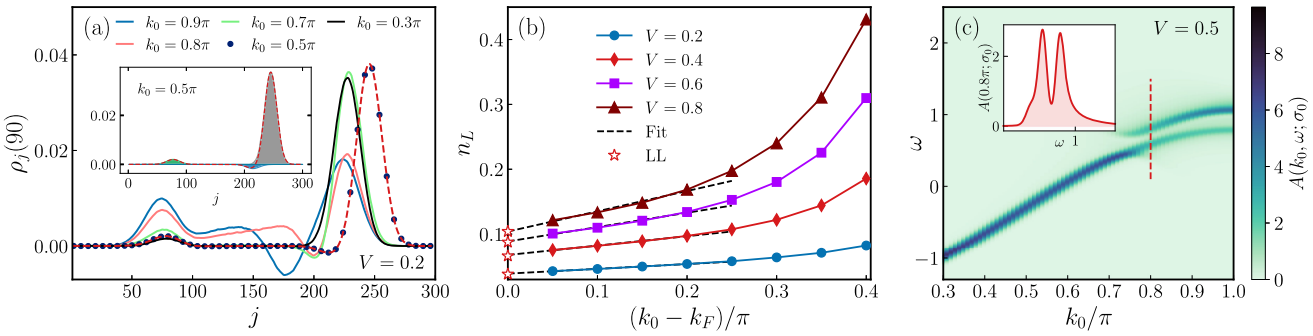

FIG. 3. Wave packet at quarter filling. (a) Averaged density profile for at fixed time $t = 90$, $V = 0.2$, and distinct values of k_0. For $k_0 = 0.5\pi$, the symbols are the tDMRG results and the dashed line is the fit to our data considering the sum of three Gaussian functions, which are shown in the inset. (b) Charge of the left-moving hump as a function of momentum for different values of V. The dashed lines represent a linear fit of the data for $(k_0 - k_F)/\pi \leq 0.2$. The stars on the vertical axis mark the LL prediction $(1 - K)/2$, valid for $k_0 \to k_F$. (c) Spectral function $A(k_0, \omega; \sigma_0)$; see Eq. (16), calculated for $V = 0.5$. The inset shows a cut for momentum $k_0 = 0.8\pi$. The peak at higher frequencies is a signature of bound states.

predicted, we have not seen any momentum dependence in $n_{R,L}$ [52]. Moreover, we observe a left-right symmetry in the low-energy humps, which is surprising since the initial wave packet at finite k_0 clearly does not have this symmetry. Last but not least, we can apply the theory also to excitations very close to the Fermi energy, i.e., $k_0 \to \pi/2$. Once $u \to v$, longer and longer times $t \gtrsim \tau_{\rm sp} \equiv \sigma_0/|v - u|$ are required to distinguish the two right-moving humps. In fact, this is in perfect agreement with conventional LL theory [6] of only one left- and one right-moving fractional charge with $(1 - K)/2$ and $(1 + K)/2$, respectively [6]. Hence, the continuous crossover from nLL to LL behavior becomes very intuitive in the dynamics of fractional charges $\gamma_{L,R}/2\pi$. In contrast, this crossover is much more involved in the frequency domain since the threshold exponents are quadratic functions of the phase shifts [26].

Quarter filling—To illustrate a more generic situation, we now consider the model in Eq. (1) at quarter filling, $k_F = \pi/4$. In this case, by solving Bethe ansatz equations, we can numerically determine the exact renormalized dispersion, Luttinger parameter, and velocity of the low-energy modes [1,50].

Figure 3(a) shows tDMRG results for $V = 0.2$ and different values of k_0 at $t = 90$ after averaging the density over four neighboring sites to smooth the $2k_F$ oscillations out. In the low-energy regime, e.g., for $k_0 = 0.3\pi$, we observe only one left and one right hump moving with velocities $\pm v$, similar to the half-filled case. However, now the charge n_L carried by the left-moving hump varies with k_0 as shown in Fig. 3(b), which in turn directly provides the momentum-dependent phase shifts $\gamma_L = 2\pi n_L$. In the extrapolation $k_0 \to k_F$ we recover the LL prediction $n_L \to (1 - K)/2$.

For larger values of k_0 [see for example $k_0 = 0.5\pi$ and 0.7π in Fig. 3(a)], the three signals predicted by the nLL are observed again: two counterpropagating charges $n_{R,L} = \kappa_{R,L}/[2\pi(u \mp v)]$ moving with velocities $\pm v$, and a large right-moving hump with velocity u. Note that the right low-energy mover carries *negative* charge since $u > v$. We again find that the time evolution of the excitation can be predicted by three propagating Gaussian wave packets [52].

As we increase the momentum, the density profile develops a complex pattern. For $k_0 = 0.8\pi$ in Fig. 3(a), the broad feature around the middle of the chain suggests the presence of additional excitations. In fact, the operator in Eq. (2) can create not only individual particles but also composite excitations with net charge $+1$. To analyze the excitations, we consider the Fourier transform of the overlap between the initial state in Eq. (2) and the time-evolved one,

$$A(k_0, \omega; \sigma_0) = \int_{-\infty}^{\infty} dt\, e^{i(\omega - E_0)t} \langle \Psi(0)|\Psi(t)\rangle, \\ = 2\pi \sum_{\alpha} |\langle \alpha|\Psi(0)\rangle|^2 \delta(\omega - E_\alpha + E_0), \qquad (16)$$

where $|\alpha\rangle$ are eigenstates of H with energy E_α above the ground-state energy E_0. In the limit $\sigma_0 \to \infty$, it reduces to the standard single-particle spectral function [55]. We compute $A(k_0, \omega; \sigma_0)$ by performing a fast Fourier transform with a cosine window in the interval $t \in [-t_{\rm max}, t_{\rm max}]$, with $t_{\rm max} = 90$.

As discussed in Ref. [55], the nLL theory for $A(k_0, \omega, \sigma_0 \to \infty)$ predicts a diverging peak at the dispersion $\omega = \varepsilon_{\rm p}$, which decays as power laws on both sides with exponents dependent on the phase shifts. In our results of $A(k_0, \omega; \sigma_0)$, this is reflected as a broad single-particle peak for $k_0 \lesssim 0.6\pi$; see Fig. 3(c). At larger momenta, $A(k_0, \omega; \sigma_0)$ displays a double-peak structure for k_0 near π, which is a clear indication of a yet unaccounted excitation in the wave packet $|\Psi(0)\rangle$ in Eq. (16). This feature is absent for half filling [52].

We identify this excitation as a composite of a two-particle bound state with a free hole as depicted in Fig. 1(c),

which has been predicted in Ref. [55]. Such a composite gives a high-energy continuum in the spectral function for momenta greater than $\pi + k_F - Q_{\rm bs}$, where $Q_{\rm bs} = [\pi - 2\arccos(V)][1 - (2k_F/\pi)]$ restricts the momentum of bound state $|\pi - k_{\rm bs}| < Q_{\rm bs}$. Note that $Q_{\rm bs}$ vanishes for $V \to 0$ or $k_F \to (\pi/2)$. In nLL theory, this type of excitation can be described by $c_j^\dagger \sim e^{-ik_0 x} B^\dagger(x) h^\dagger(x)$ [55]. For $k_0 = 0.8\pi$ in Fig. 3(a), both the bound state ($B^\dagger$) and the hole ($h^\dagger$) are created near the bottom of their respective bands. This implies a low velocity, consistent with a slow-moving hump. In general, the evolution of the wave packet may involve contributions from low- or high-energy particles, holes, and bound states that share the total momentum covered by the Gaussian distribution; see the SM [52].

Conclusions—We proposed an out-of-equilibrium protocol to investigate the fractionalization of high-energy excitations in critical chains. We clarified the crossover between LL and nLL regimes and identified contributions from elementary particles moving with different velocities and carrying fractional charges, which can be negative for $u > v$. The transport simulations reveal also more involved excitations, such as composite excitations formed by holes and bound states. This analysis also applies to quantum spin chains and spin-charge-separated quantum fluids. For the latter, spin-charge-separated quasiparticles can still be defined at finite energies [56,57], and the distinct velocities of the charge and spin channels can be directly observed in the time evolution of the charge and spin density profiles. Our work paves the way for precision tests of nLL effects through nonequilibrium dynamics in ultracold-atom platforms [58,59] and time-resolved measurements of hot electrons in quantum wires and quantum Hall edge states [60–62]. In particular, we find a fractionally charged particle with free-particle dynamics, a right-moving low-energy excitation that can be negatively charged, and a left-moving signal that gives an exact measurement of the interaction couplings in a large parameter regime. Hence, experimental measurements of counterpropagating fractional charges directly provide quantitative values of the momentum-dependent interactions in the linear and the nonlinear regimes.

Acknowledgments—This work was supported by the Deutsche Forschungsgemeinschaft (DFG, German Research Foundation)—Project No. 277625399-TRR 185 OSCAR (A4,A5), by the Conselho Nacional de Desenvolvimento Científico e Tecnológico (R. G. P.), and by a grant from the Simons Foundation (Grant No. 1023171, R. G. P.). The authors thank the high-performance cluster Elwetritsch for providing computational resources.

[1] T. Giamarchi, *Quantum Physics in One Dimension* (Clarendon Press, Oxford, 2004).
[2] F. D. M. Haldane, 'Luttinger liquid theory' of one-dimensional quantum fluids. I. Properties of the Luttinger model and their extension to the general 1D interacting spinless Fermi gas, J. Phys. C **14**, 2585 (1981).
[3] V. V. Deshpande, M. Bockrath, L. I. Glazman, and A. Yacoby, Electron liquids and solids in one dimension, Nature (London) **464**, 209 (2010).
[4] S. Tomonaga, Remarks on Bloch's method of sound waves applied to many-fermion problems, Prog. Theor. Phys. **5**, 544 (1950).
[5] J. M. Luttinger, An exactly soluble model of a many-fermion system, J. Math. Phys. (N.Y.) **4**, 1154 (1963).
[6] K.-V. Pham, M. Gabay, and P. Lederer, Fractional excitations in the Luttinger liquid, Phys. Rev. B **61**, 16397 (2000).
[7] J. M. Leinaas, M. Horsdal, and T. H. Hansson, Sharp fractional charges in Luttinger liquids, Phys. Rev. B **80**, 115327 (2009).
[8] H. Steinberg, G. Barak, A. Yacoby, L. N. Pfeiffer, K. W. West, B. I. Halperin, and K. L. Hur, Charge fractionalization in quantum wires, Nat. Phys. **4**, 116 (2007).
[9] K. Le Hur, B. I. Halperin, and A. Yacoby, Charge fractionalization in nonchiral Luttinger systems, Ann. Phys. (Amsterdam) (N. Y.) **323**, 3037 (2008).
[10] H. Kamata, N. Kumada, M. Hashisaka, K. Muraki, and T. Fujisawa, Fractionalized wave packets from an artificial Tomonaga–Luttinger liquid, Nat. Nanotechnol. **9**, 177 (2014).
[11] V. Freulon, A. Marguerite, J. M. Berroir, B. Plaçais, A. Cavanna, Y. Jin, and G. Fève, Hong-Ou-Mandel experiment for temporal investigation of single-electron fractionalization, Nat. Commun. **6**, 6854 (2015).
[12] C. Kim, A. Y. Matsuura, Z.-X. Shen, N. Motoyama, H. Eisaki, S. Uchida, T. Tohyama, and S. Maekawa, Observation of spin-charge separation in one-dimensional $SrCuO_2$, Phys. Rev. Lett. **77**, 4054 (1996).
[13] P. Segovia, D. Purdie, M. Hengsberger, and Y. Baer, Observation of spin and charge collective modes in one-dimensional metallic chains, Nature (London) **402**, 504 (1999).
[14] O. M. Auslaender, A. Yacoby, R. de Picciotto, K. W. Baldwin, L. N. Pfeiffer, and K. W. West, Tunneling spectroscopy of the elementary excitations in a one-dimensional wire, Science **295**, 825 (2002).
[15] O. M. Auslaender, H. Steinberg, A. Yacoby, Y. Tserkovnyak, B. I. Halperin, K. W. Baldwin, L. N. Pfeiffer, and K. W. West, Spin-charge separation and localization in one dimension, Science **308**, 88 (2005).
[16] B. J. Kim, H. Koh, E. Rotenberg, S.-J. Oh, H. Eisaki, N. Motoyama, S. Uchida, T. Tohyama, S. Maekawa, Z.-X. Shen, and C. Kim, Distinct spinon and holon dispersions in photoemission spectral functions from one-dimensional $SrCuO_2$, Nat. Phys. **2**, 397 (2006).
[17] M. Mourigal, M. Enderle, A. Klöpperpieper, J.-S. Caux, A. Stunault, and H. M. Rønnow, Fractional spinon excitations in the quantum Heisenberg antiferromagnetic chain, Nat. Phys. **9**, 435 (2013).

[18] T. Kinoshita, T. Wenger, and D. S. Weiss, Observation of a one-dimensional Tonks-Girardeau gas, Science **305**, 1125 (2004).

[19] B. Paredes, A. Widera, V. Murg, O. Mandel, S. Fölling, I. Cirac, G. V. Shlyapnikov, T. W. Hänsch, and I. Bloch, Tonks-Girardeau gas of ultracold atoms in an optical lattice, Nature (London) **429**, 277 (2004).

[20] G. Pagano, M. Mancini, G. Cappellini, P. Lombardi, F. Schäfer, H. Hu, X.-J. Liu, J. Catani, C. Sias, M. Inguscio, and L. Fallani, A one-dimensional liquid of fermions with tunable spin, Nat. Phys. **10**, 198 (2014).

[21] T. A. Hilker, G. Salomon, F. Grusdt, A. Omran, M. Boll, E. Demler, I. Bloch, and C. Gross, Revealing hidden antiferromagnetic correlations in doped Hubbard chains via string correlators, Science **357**, 484 (2017).

[22] A. Imambekov, T. L. Schmidt, and L. I. Glazman, One-dimensional quantum liquids: Beyond the Luttinger liquid paradigm, Rev. Mod. Phys. **84**, 1253 (2012).

[23] A. V. Rozhkov, Fermionic quasiparticle representation of Tomonaga-Luttinger Hamiltonian, Eur. Phys. J. B **47**, 193 (2005).

[24] M. Pustilnik, M. Khodas, A. Kamenev, and L. I. Glazman, Dynamic response of one-dimensional interacting fermions, Phys. Rev. Lett. **96**, 196405 (2006).

[25] M. Khodas, M. Pustilnik, A. Kamenev, and L. I. Glazman, Fermi-Luttinger liquid: Spectral function of interacting one-dimensional fermions, Phys. Rev. B **76**, 155402 (2007).

[26] A. Imambekov and L. I. Glazman, Universal theory of nonlinear Luttinger liquids, Science **323**, 228 (2009).

[27] R. G. Pereira, S. R. White, and I. Affleck, Exact edge singularities and dynamical correlations in spin-1/2 chains, Phys. Rev. Lett. **100**, 027206 (2008).

[28] V. V. Cheianov and M. Pustilnik, Threshold singularities in the dynamic response of gapless integrable models, Phys. Rev. Lett. **100**, 126403 (2008).

[29] A. Imambekov and L. I. Glazman, Exact exponents of edge singularities in dynamic correlation functions of 1D Bose gas, Phys. Rev. Lett. **100**, 206805 (2008).

[30] F. H. L. Essler, Threshold singularities in the one-dimensional Hubbard model, Phys. Rev. B **81**, 205120 (2010).

[31] R. G. Pereira, Long time correlations of nonlinear Luttinger liquids, Int. J. Mod. Phys. B **26**, 1244008 (2012).

[32] E. Bettelheim, A. G. Abanov, and P. Wiegmann, Orthogonality catastrophe and shock waves in a nonequilibrium Fermi gas, Phys. Rev. Lett. **97**, 246402 (2006).

[33] E. Bettelheim and L. Glazman, Quantum Ripples over a semiclassical shock, Phys. Rev. Lett. **109**, 260602 (2012).

[34] I. V. Protopopov, D. B. Gutman, P. Schmitteckert, and A. D. Mirlin, Dynamics of waves in one-dimensional electron systems: Density oscillations driven by population inversion, Phys. Rev. B **87**, 045112 (2013).

[35] I. V. Protopopov, D. B. Gutman, M. Oldenburg, and A. D. Mirlin, Dissipationless kinetics of one-dimensional interacting fermions, Phys. Rev. B **89**, 161104(R) (2014).

[36] G. Barak, H. Steinberg, L. N. Pfeiffer, K. W. West, L. Glazman, F. von Oppen, and A. Yacoby, Interacting electrons in one dimension beyond the Luttinger-liquid limit, Nat. Phys. **6**, 489 (2010).

[37] Y. Jin, O. Tsyplyatyev, M. Moreno, A. Anthore, W. K. Tan, J. P. Griffiths, I. Farrer, D. A. Ritchie, L. I. Glazman, A. J. Schofield, and C. J. B. Ford, Momentum-dependent power law measured in an interacting quantum wire beyond the Luttinger limit, Nat. Commun. **10**, 2821 (2019).

[38] S. Wang, S. Zhao, Z. Shi, F. Wu, Z. Zhao, L. Jiang, K. Watanabe, T. Taniguchi, A. Zettl, C. Zhou, and F. Wang, Nonlinear Luttinger liquid plasmons in semiconducting single-walled carbon nanotubes, Nat. Mater. **19**, 986 (2020).

[39] R. Senaratne, D. Cavazos-Cavazos, S. Wang, F. He, Y.-T. Chang, A. Kafle, H. Pu, X.-W. Guan, and R. G. Hulet, Spin-charge separation in a one-dimensional Fermi gas with tunable interactions, Science **376**, 1305 (2022).

[40] S. R. White and A. E. Feiguin, Real-time evolution using the density matrix renormalization group, Phys. Rev. Lett. **93**, 076401 (2004).

[41] E. A. Jagla, K. Hallberg, and C. A. Balseiro, Numerical study of charge and spin separation in low-dimensional systems, Phys. Rev. B **47**, 5849 (1993).

[42] B. Trauzettel, I. Safi, F. Dolcini, and H. Grabert, Appearance of fractional charge in the noise of nonchiral Luttinger liquids, Phys. Rev. Lett. **92**, 226405 (2004).

[43] C. Kollath, U. Schollwöck, and W. Zwerger, Spin-charge separation in cold Fermi gases: A real time analysis, Phys. Rev. Lett. **95**, 176401 (2005).

[44] T. Ulbricht and P. Schmitteckert, Is spin-charge separation observable in a transport experiment?, Europhys. Lett. **86**, 57006 (2009).

[45] K. A. Al-Hassanieh, J. Rincón, E. Dagotto, and G. Alvarez, Wave-packet dynamics in the one-dimensional extended Hubbard model, Phys. Rev. B **88**, 045107 (2013).

[46] M. Acciai, A. Calzona, G. Dolcetto, T. L. Schmidt, and M. Sassetti, Charge and energy fractionalization mechanism in one-dimensional channels, Phys. Rev. B **96**, 075144 (2017).

[47] S. Scopa, P. Calabrese, and L. Piroli, Real-time spin-charge separation in one-dimensional Fermi gases from generalized hydrodynamics, Phys. Rev. B **104**, 115423 (2021).

[48] A. Moreno, A. Muramatsu, and J. M. P. Carmelo, Charge and spin fractionalization beyond the Luttinger-liquid paradigm, Phys. Rev. B **87**, 075101 (2013).

[49] A. A. Dontsov and A. P. Dmitriev, Charge fractionalization beyond the Luttinger liquid paradigm: An analytical consideration, Phys. Rev. B **103**, 195148 (2021).

[50] V. E. Korepin, N. M. Bogoliubov, and A. G. Izergin, *Quantum Inverse Scattering Method and Correlation Functions* (Cambridge University Press, Cambridge, England, 1993).

[51] R. Shankar, *Principles of Quantum Mechanics* (Springer, New York, 1994).

[52] See Supplemental Material at http://link.aps.org/supplemental/10.1103/PhysRevLett.133.086502 for a detailed analysis of the free fermion wave packet, the spectral function at half filling, and the momentum-dependent charge of the left-moving hump at quarter filling.

[53] Y. Tsukamoto, T. Fujii, and N. Kawakami, Critical behavior of Tomonaga-Luttinger liquids with a mobile impurity, Phys. Rev. B **58**, 3633 (1998).

[54] L. Balents, X-ray-edge singularities in nanotubes and quantum wires with multiple subbands, Phys. Rev. B **61**, 4429 (2000).

[55] R. G. Pereira, S. R. White, and I. Affleck, Spectral function of spinless fermions on a one-dimensional lattice, Phys. Rev. B **79**, 165113 (2009).

[56] T. L. Schmidt, A. Imambekov, and L. I. Glazman, Fate of 1D spin-charge separation away from Fermi points, Phys. Rev. Lett. **104**, 116403 (2010).

[57] F. H. L. Essler, R. G. Pereira, and I. Schneider, Spin-charge-separated quasiparticles in one-dimensional quantum fluids, Phys. Rev. B **91**, 245150 (2015).

[58] P. L. Pedersen, M. Gajdacz, N. Winter, A. J. Hilliard, J. F. Sherson, and J. Arlt, Production and manipulation of wave packets from ultracold atoms in an optical lattice, Phys. Rev. A **88**, 023620 (2013).

[59] J. Vijayan, P. Sompet, G. Salomon, J. Koepsell, S. Hirthe, A. Bohrdt, F. Grusdt, I. Bloch, and C. Gross, Time-resolved observation of spin-charge deconfinement in fermionic Hubbard chains, Science **367**, 186 (2020).

[60] M. Kataoka, N. Johnson, C. Emary, P. See, J. P. Griffiths, G. A. C. Jones, I. Farrer, D. A. Ritchie, M. Pepper, and T. J. B. M. Janssen, Time-of-flight measurements of single-electron wave packets in quantum Hall edge states, Phys. Rev. Lett. **116**, 126803 (2016).

[61] M. Hashisaka, N. Hiyama, T. Akiho, K. Muraki, and T. Fujisawa, Waveform measurement of charge- and spin-density wavepackets in a chiral Tomonaga-Luttinger liquid, Nat. Phys. **13**, 559 (2017).

[62] C. Bäuerle, D. C. Glattli, T. Meunier, F. Portier, P. Roche, P. Roulleau, S. Takada, and X. Waintal, Coherent control of single electrons: A review of current progress, Rep. Prog. Phys. **81**, 056503 (2018).